NASA/TM—2003-212327

ARL–TR–2958

Spiral Bevel Pinion Crack Detection in a Helicopter Gearbox

Harry J. Decker and David G. Lewicki
U.S. Army Research Laboratory, Glenn Research Center, Cleveland, Ohio

June 2003

The NASA STI Program Office . . . in Profile

Since its founding, NASA has been dedicated to the advancement of aeronautics and space science. The NASA Scientific and Technical Information (STI) Program Office plays a key part in helping NASA maintain this important role.

The NASA STI Program Office is operated by Langley Research Center, the Lead Center for NASA's scientific and technical information. The NASA STI Program Office provides access to the NASA STI Database, the largest collection of aeronautical and space science STI in the world. The Program Office is also NASA's institutional mechanism for disseminating the results of its research and development activities. These results are published by NASA in the NASA STI Report Series, which includes the following report types:

- TECHNICAL PUBLICATION. Reports of completed research or a major significant phase of research that present the results of NASA programs and include extensive data or theoretical analysis. Includes compilations of significant scientific and technical data and information deemed to be of continuing reference value. NASA's counterpart of peer-reviewed formal professional papers but has less stringent limitations on manuscript length and extent of graphic presentations.

- TECHNICAL MEMORANDUM. Scientific and technical findings that are preliminary or of specialized interest, e.g., quick release reports, working papers, and bibliographies that contain minimal annotation. Does not contain extensive analysis.

- CONTRACTOR REPORT. Scientific and technical findings by NASA-sponsored contractors and grantees.

- CONFERENCE PUBLICATION. Collected papers from scientific and technical conferences, symposia, seminars, or other meetings sponsored or cosponsored by NASA.

- SPECIAL PUBLICATION. Scientific, technical, or historical information from NASA programs, projects, and missions, often concerned with subjects having substantial public interest.

- TECHNICAL TRANSLATION. English-language translations of foreign scientific and technical material pertinent to NASA's mission.

Specialized services that complement the STI Program Office's diverse offerings include creating custom thesauri, building customized databases, organizing and publishing research results . . . even providing videos.

For more information about the NASA STI Program Office, see the following:

- Access the NASA STI Program Home Page at ***http://www.sti.nasa.gov***

- E-mail your question via the Internet to help@sti.nasa.gov

- Fax your question to the NASA Access Help Desk at 301–621–0134

- Telephone the NASA Access Help Desk at 301–621–0390

- Write to:
  NASA Access Help Desk
  NASA Center for AeroSpace Information
  7121 Standard Drive
  Hanover, MD 21076

NASA/TM—2003-212327

ARL–TR–2958

Spiral Bevel Pinion Crack Detection in a Helicopter Gearbox

Harry J. Decker and David G. Lewicki
U.S. Army Research Laboratory, Glenn Research Center, Cleveland, Ohio

Prepared for the
59th Annual Forum and Technology Display
sponsored by the American Helicopter Society
Phoenix, Arizona, May 6–8, 2003

National Aeronautics and
Space Administration

Glenn Research Center

June 2003

The Propulsion and Power Program at
NASA Glenn Research Center sponsored this work.

Available from

NASA Center for Aerospace Information
7121 Standard Drive
Hanover, MD 21076

National Technical Information Service
5285 Port Royal Road
Springfield, VA 22100

Available electronically at http://gltrs.grc.nasa.gov

Spiral Bevel Pinion Crack Detection in a Helicopter Gearbox

Harry J. Decker and David G. Lewicki
U.S. Army Research Laboratory
National Aeronautics and Space Administration
Glenn Research Center
Cleveland, Ohio 44135
E-mail: Harry.J.Decker@grc.nasa.gov, David.G.Lewicki@grc.nasa.gov

ABSTRACT

The vibration resulting from a cracked spiral bevel pinion was recorded and analyzed using existing Health and Usage Monitoring System (HUMS) techniques. A tooth on the input pinion to a Bell OH-58 main rotor gearbox was notched and run for an extended period at severe over-torque condition to facilitate a tooth fracture. Thirteen vibration-based diagnostic metrics were calculated throughout the run. After 101.41 hours of run time, some of the metrics indicated damage. At that point a visual inspection did not reveal any damage. The pinion was then run for another 12 minutes until a proximity probe indicated that a tooth had fractured. This paper discusses the damage detection effectiveness of the different metrics and a comparison of effects of the different accelerometer locations.

INTRODUCTION

Since 1988, the NASA Glenn Research Center has been working on improving gear damage detection using vibration monitoring. Most of the effort has focused on pitting and other surface distress failures. Later, the testing expanded into oil debris monitoring-based HUMS, vibration-based crack detection, and data fusion. Gear cracks, although potentially more catastrophic, are much less common, thus more difficult to study.

There have been several studies [1-6] to determine the onset of a gear tooth fracture in a helicopter gearbox. Some of these studies have been planned and others have been the result of unplanned faults. There have been few attempts to detect a fracture at its onset and then simulate a mission profile in order to determine the remaining life of the component.

There have been studies on gear fault detection for a spiral bevel pinion [7-9]. These studies have primarily focused on the surface contact mode of failure (pitting). The higher contact ratio of a spiral bevel pinion makes the detection of a small fault even more difficult. Some argue that the metrics that are readily available are sufficient to detect, and even in some cases, predict the remaining life of the gear.

The objective of this study was to evaluate vibration-based diagnostic metric to detect gear crack initiation. To accomplish this, seeded fault tests were conducted using a helicopter main rotor transmission. Various over-torque conditions were run to facilitate crack initiation. A visual inspection was performed before each change in torque.

FAULT DETECTION METHODS

Thirteen metrics that are available in the open literature were evaluated in this study. They were applied to the vibration signals of a relatively simple helicopter main rotor gearbox.

All of the diagnostic techniques discussed in this paper require time synchronous averaging. Time synchronous averaging has two desirable effects: (1) it reduces the effects of items in the vibration signal that are not synchronous with shaft and mesh frequencies; (2) because of this, the amplitudes of the desired parts of the signal are effectively amplified relative to the noise.

A once per revolution tachometer pulse is required to synchronize different parts of the vibration signal. The tachometer signal is used to divide the digitized vibration signal into blocks representing exactly one revolution of the gear being studied. The beginning and end data points are interpolated to provide more accurate and consistent averages. Each block's data record is then interpolated to provide a convenient number of equally spaced points (typically a power of two, such as 1024) for the feature detection and extraction process. By interpolating each revolution into an equal number of points, slight changes in the rotational speed can be accommodated. Since each point in the signal now refers to the same angular position for all the sampled rotations, the blocks are simply averaged. A simple linear average is used since experience has shown that the interpolation method is not significant [10].

The traditional methods of gear failure detection methods are typically based on some statistical measurement of vibration energy. The primary differences are based on which of the characteristic frequencies are included, excluded, or used as a reference [11].

Root Mean Square

The root mean square (RMS) is defined to be the square root of the average of the sum of the squares of an infinite number of samples of the signal (Equation 1). It is also sometimes referred to as the standard deviation of the signal average. For a simple sine wave, the RMS value will be defined to be approximately 0.707 times the amplitude of the signal.

$$RMS = \sqrt{\frac{1}{N}\left[\sum_{i=1}^{N}(S_i)^2\right]} \tag{1}$$

Crest Factor

The Crest Factor (CF), shown in Equation 2, is calculated by dividing the maximum positive peak value by the RMS value of the signal [12]. This makes the metric a normalized measurement of the amplitude of the signal. A signal that has a few, high amplitude peaks would produce a greater Crest Factor as the numerator would increase (high amplitude peaks), as the denominator decreases (few peaks means lower RMS).

$$CF = \frac{S_{0-pk}}{RMS} \tag{2}$$

Energy Operator

For the Energy Operator [13], the input signal for each point in time is squared and the product of the point before and after is subtracted. In the case of the endpoints, the data is looped around. Specifically, when calculating the first point, use the last point and vice versa. The normalized kurtosis of the resultant signal is then taken and reported as the energy operator.

Kurtosis

The kurtosis (Equation 3) is simply the normalized fourth moment of the signal [14]. The moment is normalized to the square of the variance of the signal. The kurtosis is a statistical measure of the number and amplitude of peaks in a signal. That is, a signal that has more and sharper peaks will have a larger value. A Gaussian distribution has a kurtosis value of very nearly three. It should be noted that some investigators subtract 3 from this calculated value.

$$\text{Kurtosis} = \frac{N\sum_{i=1}^{N}(S-\bar{S})^4}{\left[\sum_{i=1}^{N}(S-\bar{S})^2\right]^2} \tag{3}$$

where

S	signal
$\bar{S}$	mean value of signal
i	data point number in time record
N	number of data points

Energy Ratio

Heavy uniform wear can be detected by the energy ratio [12]. The difference signal (d) is the resultant signal after the regular meshing components (r) (mesh and harmonic frequencies) are removed. It compares the energy contained in the difference signal to the energy contained in the regular components signal. The theory is that as wear progresses, the energy is moved from the regular signal to the difference signal (Equation 4).

$$ER = \frac{RMS_d}{RMS_r} \tag{4}$$

M6A

The M6A metric [15], shown in Equation 5, is a continuation of the kurtosis. In this particular case, it is the sixth moment that is used. It is normalized in a similar manner as the kurtosis, except that the variance now has to be raised to the third power. In general, the characteristics of the spread of the distribution show up to be even (as opposed to odd) functions of the statistical moment. The odd functions relate the position of the peak density distribution with respect to the mean.

$$M6 = \frac{N^2\sum_{i=1}^{N}(d-\bar{d})^6}{\left[\sum_{i=1}^{N}(d-\bar{d})^2\right]^3} \tag{5}$$

where

d	difference signal
$\bar{d}$	mean value of difference signal
i	data point number in time record
N	number of data points

FM4

The FM4 vibration diagnostic metric (Equation 6) is one of the most popular metrics used [16]. This metric detects changes in the vibration resulting from damage limited to several teeth. The FM4 metric is non-dimensional and is calculated by dividing the fourth statistical moment about the mean by the square of the variance of the difference. As long as damage propagates locally, the FM4 metric will

increase. When damage starts becoming generalized, the value decreases.

$$FM4 = \frac{N\sum_{i=1}^{N}(d_i - \bar{d})^4}{\left[\sum_{i=1}^{N}(d_i - \bar{d})^2\right]^2} \quad (6)$$

where

- d difference signal
- $\bar{d}$ mean value of difference signal
- N total number of points in time record
- I data point number in time record

NA4

The NA4 metric (Equation 7) was developed to overcome a shortcoming of the FM4 metric [11]. As the occurrences of damage progresses in both number and severity, FM4 becomes less sensitive to the new damage. Two changes were made to the FM4 metric to develop the NA4 metric as one that is more sensitive to progressing damage. One change is that FM4 is calculated from the difference signal while NA4 is calculated from the residual signal. The residual signal includes the first order sidebands that were removed from the difference signal. The second change is that trending was incorporated into the NA4 metric. While FM4 is calculated as the ratio of the kurtosis of the data record divided by the square of the variance of the same data record, NA4 is calculated as the ratio of the kurtosis of the data record divided by the square of the average variance. The average variance is the mean value of the variance of all previous data records in the run ensemble. These two changes make the NA4 metric a more sensitive and robust metric. The NA4 metric is calculated by

$$NA4 = \frac{N\sum(r_i - \bar{r})^4}{\frac{1}{M}\sum_j\left[\sum_i(r_{ij} - \bar{r}_j)^2\right]^2} \quad (7)$$

where

- r residual signal
- $\bar{r}$ mean value of residual signal
- N total number of points in time record
- M current time record in run ensemble
- i data point number in time record
- j time record number in run ensemble

NB4

The NB4 metric is the time-averaged kurtosis of the envelope of the signal that is bandpass filtered about the mesh frequency [17]. An estimate of the amplitude modulation caused by the sidebands of the mesh frequency, is calculated using the Hilbert Transform. The Hilbert transform creates a complex time signal in which the real part is the bandpassed signal and the imaginary part is the Hilbert transform of the signal.

NA4*

As damage progresses from being localized to distributed, the variance of the kurtosis increases dramatically. Since the kurtosis is normalized by the variance, this results in the kurtosis decreasing to normal values even with damage present. To counter this effect, NA4* was developed [18]. While the kurtosis for a data record is normalized by the squared average variance for the run ensemble for NA4, with NA4* the kurtosis for a data record is normalized by the squared variance for a gearbox in good condition. This is a change in the trending of the data and was proposed to make a metric that is more robust as damage progresses.

In order to estimate the variance for a gearbox in good condition, a minimum number of data records of a run ensemble is chosen to ensure a statistically significant sample size. The variance of the residual signal for all data records is calculated, as well as the mean and standard deviation. The mean is used as the current estimate of the variance for a gearbox in good condition. When the next data record is available, a judgment is made as to whether to include that data record as representative of a good gearbox. A gearbox with damaged gears will have a larger variance that one in good condition. The decision is based on an upper limit L (Equation 8), which in turn is dependent on the choice of a probability coefficient Z, and is calculated by

$$L = \bar{x} + \frac{Z}{\sqrt{n}}\sigma \quad (8)$$

where

- $\bar{x}$ mean value of previous variances
- Z value for a normal distribution
- σ standard deviation of previous variances
- n number of samples ($n \geq 30$)

The value for the Z parameter can be found in introductory statistics books. If the current variance exceeds this limit, then it is judged that the gearbox is no longer in "good" condition and the previous estimate of the variance is used for the remainder of the run ensemble. If the variance for the new data record does not exceed this limit, then the new data record is included into the data representing the gearbox in good condition.

The decision of what probability coefficient is chosen is based on many factors. The most difficult trade-off is that of Type I or Type II errors. A Type I errors is an undetected

defect. A Type II error, on the other hand, reports damage when none is present. The choice of the probability coefficient is a compromise between having too many Type II errors and not detecting damage.

M6A*

This metric is based on the M6A metric with the exception that it includes the averaging effect of NA4* and the variance comparison present in the denominator.

FM4*

The diagnostic metric FM4*metric is, like NB4*, the addition of the run ensemble averaging and the statistical limitation of the growth of the square of the variance. The calculation of the numerator of this metric remains the same as in FM4. The denominator has the averaging effect of NA4*, and also determines if the current variance is of sufficient probability to be contained in the previous samples.

NB4*

The diagnostic metric NB4* is the addition of the run ensemble averaging and the statistical limitation of the growth of the square of the variance first introduced in the development of NA4*. The calculation of the numerator of this metric remains the same as in NB4. The denominator does have the averaging effect of NA4*, and determines if the current variance is of sufficient probability to be contained in the previous samples.

EXPERIMENT CONFIGURATION

OH-58 Main Rotor Transmission

The OH-58 is a single-engine, land-based, light, observation helicopter. The helicopter serves both military (OH-58 Kiowa) and commercial (Bell Model 206 Jet Ranger) needs. The design maximum torque and speed for the OH-58A main-rotor transmission (Figure 1) is 350 N-m (3100 in-lb) input torque and 6060 rpm input speed [19]. This corresponds to 222 kW (298 HP). The transmission is a two-stage reduction gearbox. The first stage is a spiral bevel gear set with a 19-tooth pinion that meshes with a 71-tooth gear. Triplex ball bearings and one roller bearing support the bevel-pinion shaft. Duplex ball bearings and one roller bearing support the bevel-gear shaft in an overhung configuration.

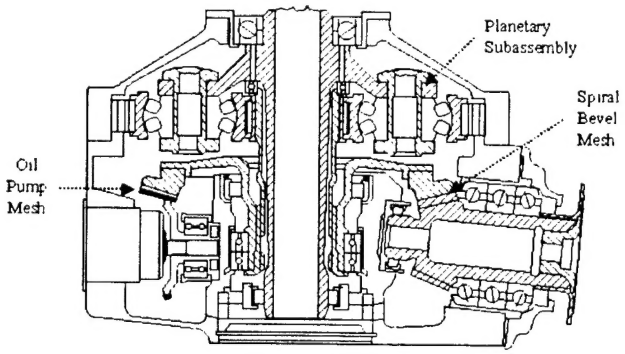

Figure 1. OH-58 Main Rotor Transmission

A planetary mesh provides the second reduction stage. The bevel-gear shaft is splined to a sun gear shaft. The 27-tooth sun gear drives three or four 35-tooth planet gears, depending on the model. The planet gears mesh with a 99-tooth fixed ring gear splined to the transmission housing. Power is taken out through the planet carrier splined to the output mast shaft. The output shaft is supported on top by a split-inner-race ball bearing and on the bottom by a roller bearing. The overall reduction ratio of the main power train is 17.44:1.

The 71-tooth bevel gear also drives a 27-tooth accessory gear. The accessory gear runs an oil pump, which supplies lubrication through jets and passageways located in the transmission housing.

NASA 500 HP Helicopter Transmission Test Stand

The OH-58 transmission was tested in the NASA Glenn 500 HP Helicopter Transmission Test Stand (Figure 2). The test stand operates on the closed-loop, or torque-regenerative, principle. Mechanical power circulates through a closed loop of gears and shafts, one of which is the test transmission. The output of the test transmission attaches to the bevel gearbox, whose output shaft passes through a hollow shaft in the closing-end gearbox and connects to the differential gearbox. The output of the differential attaches to the hollow shaft in the closing-end gearbox. The output of the closing-end gearbox connects to the input of the test transmission, thereby closing the loop.

A 149-kW (200 HP) variable speed direct-current (DC) motor powers the test stand and controls the speed. The motor output attaches to the closing-end gearbox. Since power circulates around the loop, the motor replenishes only friction losses.

An 11-kW (15 HP) DC motor provides the torque in the closed loop. The motor drives a magnetic particle clutch. For the OH-58 application, the clutch output does not turn but exerts a torque. This torque transfers through a speed-reducer gearbox and a chain drive to a large sprocket on the differential gearbox. The torque on the sprocket puts a torque in the closed loop by displacing the gear attached to the bevel gearbox output shaft with the gear connected to the input shaft of the closing-end gearbox. This is done within the differential gearbox by a compound planetary system where the planet carrier attaches to the sprocket housing.

The magnitude of torque in the loop is adjusted by changing the electric field strength of the magnetic particle clutch. For applications other than the OH-58 transmission where the speed ratio of the test transmission is slightly different or when slippage occurs (i.e., traction drives), the planet/ sprocket/chain assembly rotates to make up for the speed mismatches that occur in the closed loop.

A mast-shaft loading system in the test stand simulates rotor loads imposed on the OH-58 transmission output mast shaft. The OH-58 transmission output mast shaft connects to a loading yoke. Two vertical load cylinders connected to the yoke produce lift loads. A single horizontal load cylinder connected to the yoke produces shear loads. A 13,790-kPa (2000-psig) gas nitrogen system powers the cylinders. Pressure regulators connected to each loading cylinder's nitrogen supply adjust the magnitude of lift and shear forces.

The test transmission input and output shafts have speed sensors, torquemeters, and slip rings. All three load cylinders on the mast yoke are mounted to load cells. The test transmission internal oil pump supplies lubrication. An external oil-water heat exchanger cools the test transmission oil.

The 149-kW (200 HP) motor has a speed sensor and a torquemeter. The magnetic particle clutch has speed sensors and thermocouples on the input and output shafts. A facility oil-pumping and cooling system lubricates the differential gearbox, the closing-end gearbox, and the bevel gearbox. The facility gearboxes have accelerometers, thermocouples, and chip detectors, for health and condition monitoring.

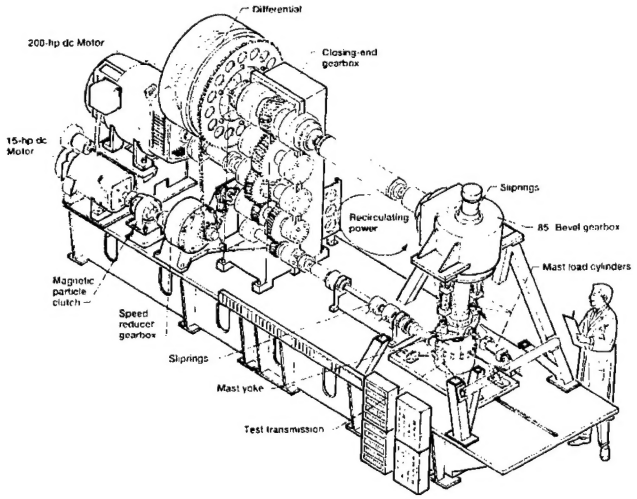

Figure 2. 500 HP Helicopter Transmission Test Stand

Test Gear

The spiral bevel pinion has 19 teeth, a diametral pitch of 6.940 teeth/inch, a face width of 1.28 inch, a bevel angle of 15 degrees 16 minutes, and a spiral angle of 30 degrees left hand, clockwise. It meshes with a 71 tooth gear to form the first stage of reduction. Triplex ball bearings and one roller bearing support the pinion.

Notch Geometry

A notch was machined into the fillet region of one spiral bevel pinion tooth using electro-discharge machining. The dimensions were approximately 0.1 inch wide, 0.005 inch tall and 0.005 inch deep. After a significant amount of run time at extreme torques, it was determined that the notch was not of sufficient size to facilitate crack initiation. A second notch (Figure 3) was machined in the same area and measured 0.12 inch wide by 0.01 inch tall by 0.08 inch deep. This notch geometry was sufficient to initiate a crack although an extreme over-torque condition was required.

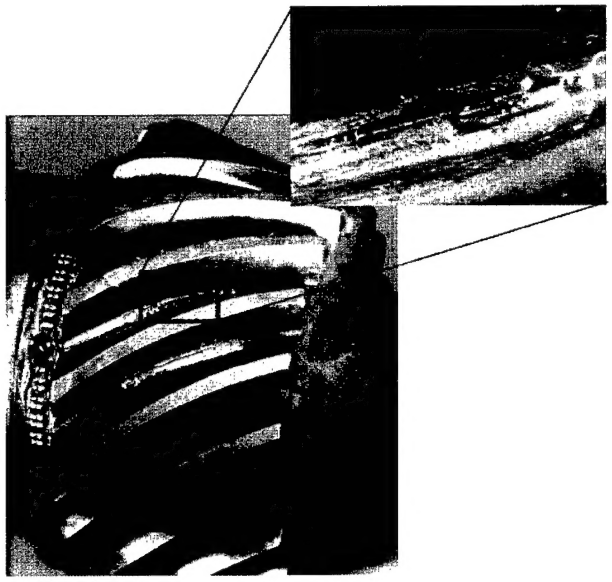

Figure 3. Photograph of notch

Sensors

A suite of sensors were mounted to facilitate the detection of crack initiation and propagation. It consisted of a tachometer, five accelerometers, and a proximity probe.

The once per revolution tachometer signal is generated using an infrared optical sensor that is located on the input shaft to the test gearbox. The sensor detects a change in the reflectivity of an infrared light. The connecting shaft has a piece of highly reflective silver colored tape cemented to the black oxide coated shaft. This provides a reliable signal that has good dynamic performance.

The five accelerometers were located at various locations around the gearbox as shown in Figure 4. Accelerometer 1 is located on the input bevel gear housing immediately

above where the input shaft connects to the pinion and is oriented to be most responsive in the vertical direction. Accelerometer 2 is at the same location and is aligned to the rotational axis of the input shaft. Accelerometers 3 and 4 are mounted around the circumference of the ring gear housing and are located 45 and 225 degrees from the input pinion gear. Accelerometer 5 is mounted to one of the attachment bolts near accelerometer 4. Accelerometers 3, 4, and 5 are mounted in the axial-transverse plane and have sensitivities in both directions. The accelerometers are linear to 20 kHz and have a resonance frequency of 90 kHz.

Accelerometer positions 1, 2, and 3 were chosen based on previous experience [20]. In previous testing, accelerometers 1 and 2 had the spiral bevel harmonics as the dominant components. Accelerometer 3 produced the highest levels of vibration where the dominant vibration sources were the spiral bevel mesh and the planetary mesh. Accelerometer locations 4 and 5 also had significant spiral bevel mesh frequency components. The transfer path through the ring gear provides an excellent source for gear mesh vibrations.

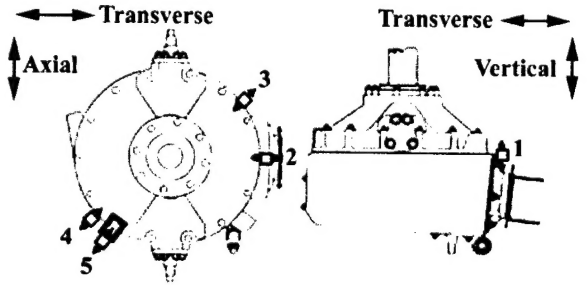

Figure 4. Accelerometer locations

A radio frequency (RF) eddy current proximity probe was mounted inside the transmission on one of the support webs. The probe coil radiates a small RF field near the tip of the probe. If there is no conductive material within this field, there is no power loss in the RF signal. When the top land of the pinion approaches the probe tip, eddy currents are generated on the surface of the pinion, resulting in a power loss in the RF signal. This allows the proximity probe to detect the passing of the top land of the teeth.

Test Procedure

The pinion was run at the design speed of 6060 rpm and at percentages of the maximum design torque according to Figure 5. The goal was to initiate a crack in the pinion at the lowest possible torque. Thus, the pinion was initially run at 80% toque. The torque was gradually increased. The inverted triangles represent the periods where an inspection occurred. Inspections were visual using a 60X microscope. At 80 hours run time, the notch was deepened (solid square symbol). This paper deals with the vibration acquired during the last 150% torque cycle between 97 hours runtime and the end of the test.

The vibration, speed and proximity probe signals were passed through a low-pass elliptical anti-aliasing filter with a cutoff frequency of 56 kHz. This data was then acquired using a personal computer equipped with a analog to digital converter capable of digitizing 8 channels at 150 kHz each. A record length of 1.5 seconds was taken every 15 seconds and analyzed. The analysis was performed and displayed near real time.

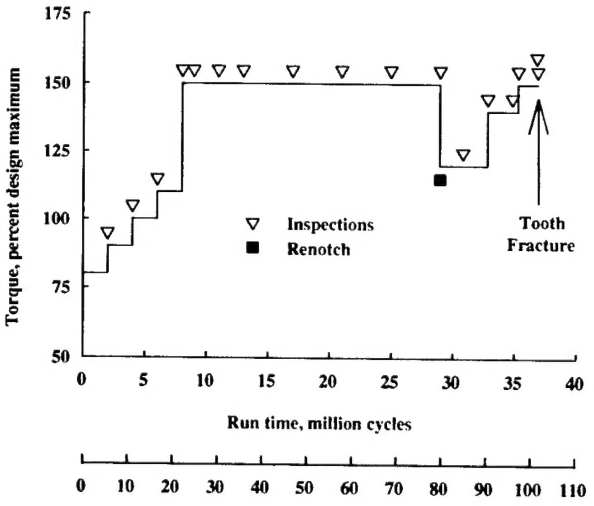

Figure 5. Loading history of pinion

RESULTS

From the vibration data, there was an indication of potential damage at 101.15 hours run time. A visual inspection with a 60X microscope was performed after 101.41 hours and no crack initiation was detected. The pinion was reinstalled into the gearbox and run for another 12 minutes until the proximity probe indicated a spike corresponding to damage to one of the teeth. Upon disassembly, a tooth was found to be fractured off as shown in Figure 6. The proximity probe had detected the missing top land when the signal caused by the passing of the damaged tooth produced a differing output signal. The fractured tooth was the one with the notch. Close examination shows that the notch surfaces were evenly distributed between the two pieces.

Detailed analysis of the proximity probe data indicates that at 101.4723 hours of run time (approximately 9 minutes before complete fracture), a once per revolution spike was

continuously observed. The most probable explanation for this is that at this point massive deflection was taking place. At 101.621 hours into the test, the damaged tooth separated from the remainder of the gear.

It is believed that the pinion was cracked at the 101.15 hour run time inspection. It is also believed that the crack was not visually detected due to two factors. First, adhesive from strain gages installed in the pinion tooth root could have masked the surface to affect the visual inspection. Second, the pinion was inspected under no load and might require tension to open the crack for successful visual inspection.

The RMS of the time synchronous average is shown in Figure 7. Brief periods of the run encountered torque fluctuations (between 98.3964 and 98.4931 hours of run time). The exact cause of the fluctuations are unknown, but the may have been caused by facility electrical power variations or instrumentation noise. The RMS was very sensitive to the torque fluctuations. Overall, there was no definitive indication of damage from the RMS metric except for at the end of the run where tooth fracture occurred.

The Crest Factor in Figure 8 shows apparent damage. This indication of damage is after the shutdown and inspection which was prompted by other metrics. This metric is not as sensitive to the torque spikes as was the RMS

The responsiveness of the Energy Operator (Figure 9) to the torque spikes casts some uncertainty to its ability to detect the onset of damage. Once the damage has progressed, it becomes a good metric as its value does not decrease to a value indicative of an undamaged state.

Figure 6. Photograph of fracture

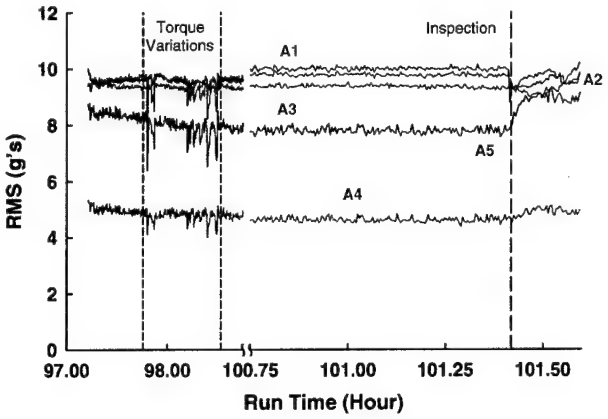

Figure 7. RMS of Synchronous Average

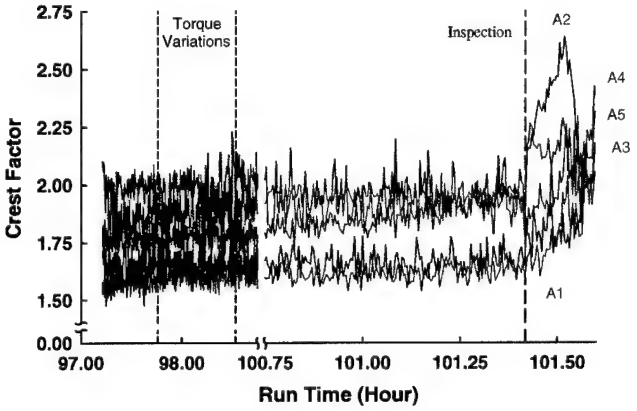

Figure 8. Crest Factor

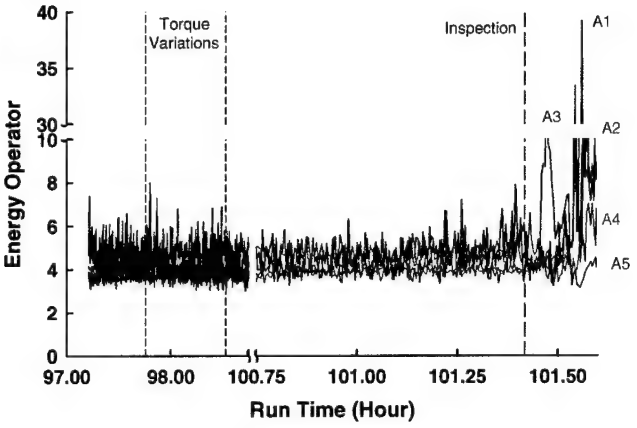

Figure 9. Energy Operator

The Kurtosis (Figure 10) is one of the most responsive of the metrics to the torque fluctuations early in the run. There is some possible indication of damage before the shutdown. This is tempered by the sensitivity to outside influences. Once the damage has progressed, there is an absolute indication of damage.

Figure 11 shows how the responsiveness to the torque spikes makes the Energy Ratio less useful. The uncertainty caused by the torque excursions cast doubt on the metric's suitability until well after other metrics have demonstrated the existence of damage.

The M6A metric (Figure 12) shows less response to the torque fluctuations and exhibits a general upward trend starting almost 30 minutes before shut down and inspection. Once the damage has become a total fracture, the metric shows a definite upset from its normal value.

The torque fluctuations did not have a significant effect on the FM4 metric (Figure 13). There is some gradual upward trending of the metric starting at about 3.5 hours into the run. The real indication of damage occurs after the inspection. This metric also shows one of the potential drawbacks of many of the metrics in its ability to return to a value indicative of a no fault condition.

The metric that best provided indication that damage was occurring or imminent was NA4 (Figure 14). It appears to have indicated damage 15 minutes before the shutdown or 35 minutes before the loss of the tooth. Unfortunately, the torque excursions have a tendency to reduce the confidence in this metric until other metrics confirm the existence of damage.

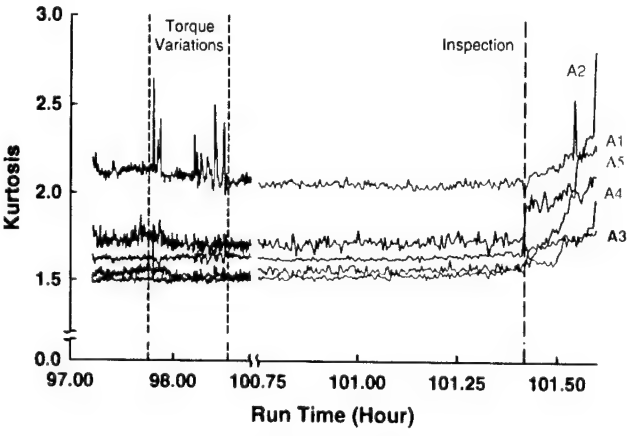

Figure 10. Kurtosis

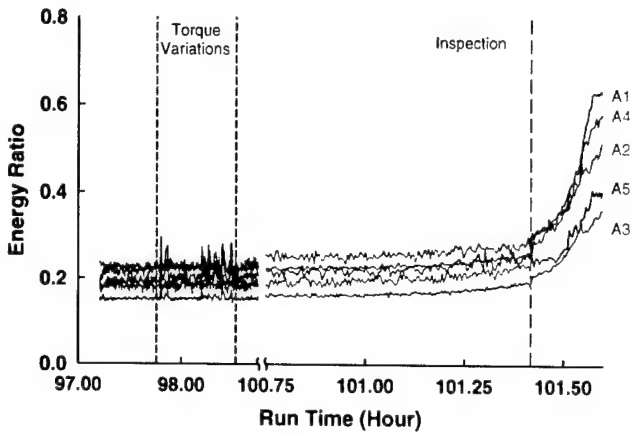

Figure 11. Energy Ratio

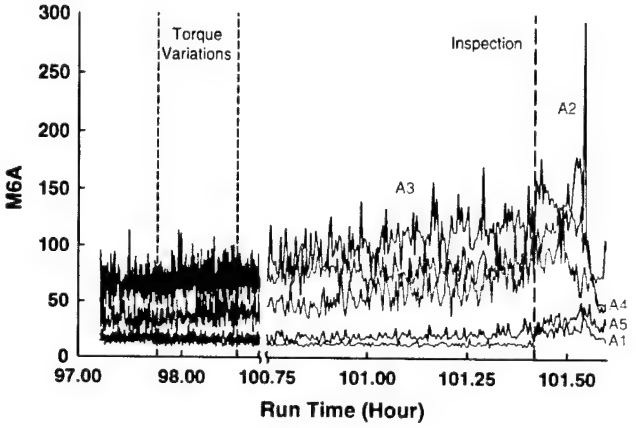

Figure 12. M6A

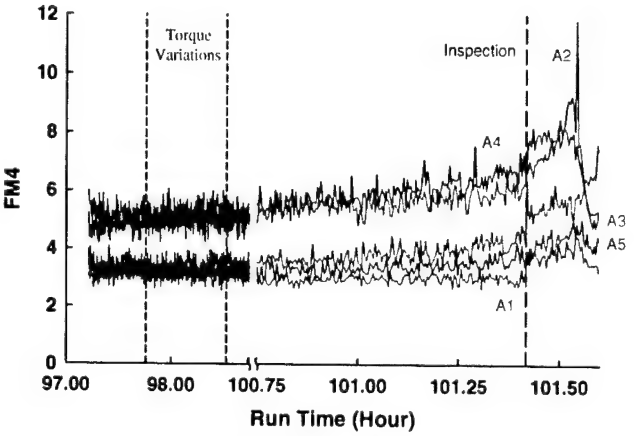

Figure 13. FM4

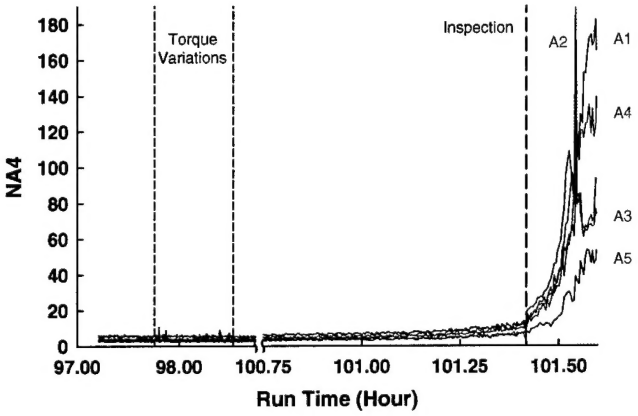

Figure 14. NA4

The NB4 metric (Figure 15) did not exhibit any of the detrimental torque sensitivities of some of the other metrics. It also only started to indicate damage about 4.8 minutes before the inspection shutdown. The stability of the metric during the run does tend to increase its usefulness. The metric also had a definite response to the actual damage.

The NA4* metric (Figure 16) exhibited a time delay relative to the NA4 metric on which it is based. The metric was designed to be more responsive. It also appeared to be more responsive to torque fluctuations than NA4.

Figure 17 shows the M6A* metric. This metric displays the undesirable characteristic of being too responsive to torque variations and also returning to a condition that can be misconstrued as being in a no damage condition.

The FM4* metric (Figure 18) was only slightly responsive to the torque fluctuations. It did appear to reveal that damage was occurring before the shutdown and inspection. After restarting the test, the metric responded in a manner that gave no doubts about whether there was damage or not.

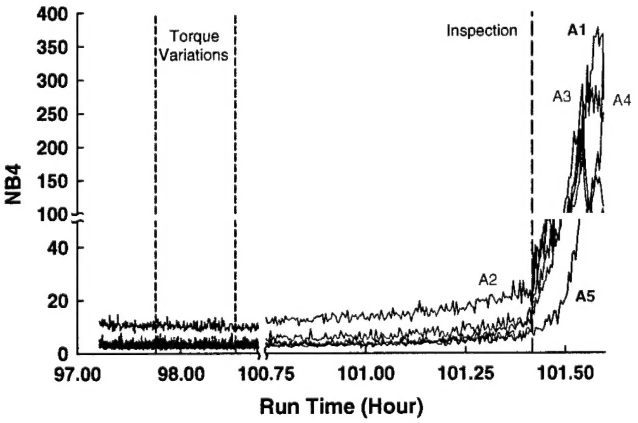

Figure 15. NB4

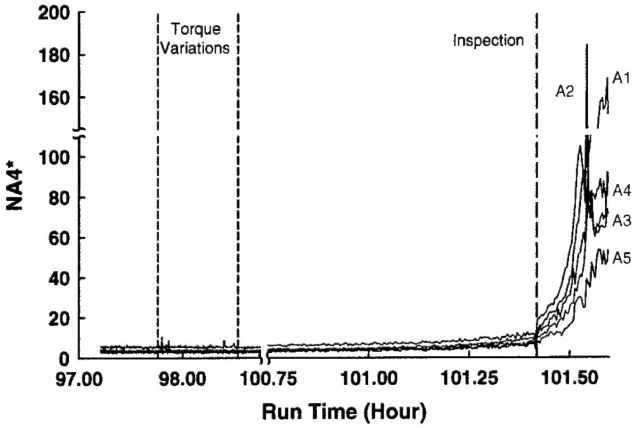

Figure 16. NA4*

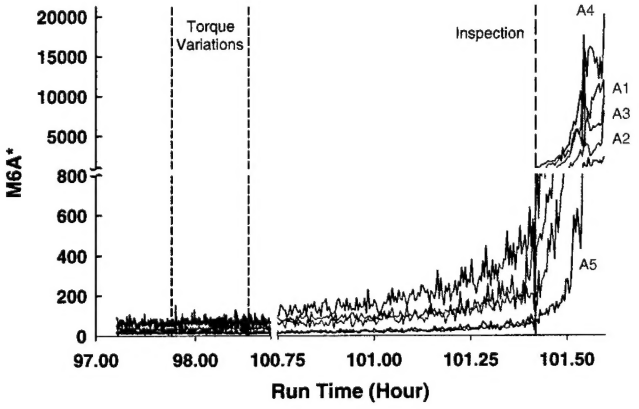

Figure 17. M6A*

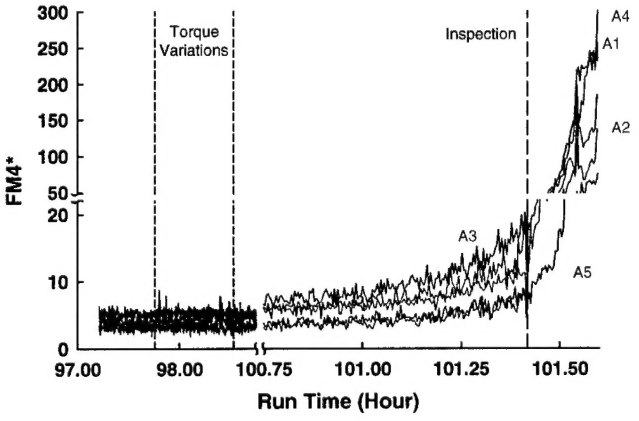

Figure 18. FM4*

The NB4* metric (Figure 19) is much like the NB4 metric in that it is relatively insensitive to torque while still responding to damage nicely.

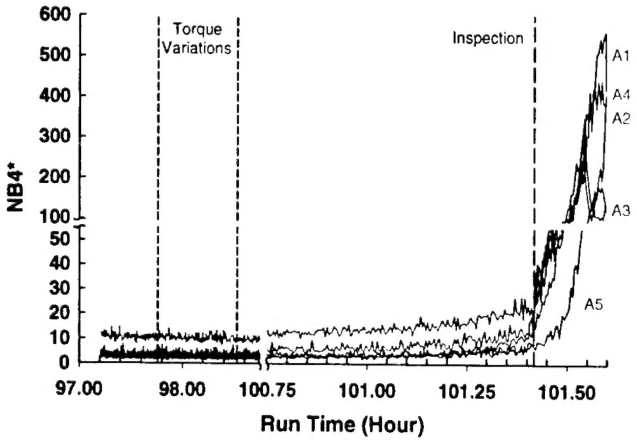

Figure 19. NB4*

If the contributions from each of the accelerometers are examined and compared, it is interesting to note that the A1 and A5 accelerometers provided the least information. Specifically, these accelerometers provided indication of damage after the other accelerometers. The A1 accelerometer is the only one that is most sensitive in the vertical direction. The A5 accelerometer was the only accelerometer that was mounted in a different manner and resulted did not have a major effect on any of the metrics. This may be due to the mounting block that was used.

The A2, A3 and A4 accelerometers produced the majority of the remaining best responses. It is interesting to note that these accelerometers all have their primary sensitivities with a component aligned in the axial direction. A2 is primarily axial in direction and located on the most direct path. This would account for its high degree of performance. A3 and A4 both provided significant indication of damage, but due to their more distant location from the pinion mesh, their signals were most likely more attenuated.

CONCLUSIONS

This study evaluated vibration-based diagnostic metric to detect gear crack initiation. Seeded fault tests were conducted using a helicopter main rotor transmission. Various over-torque conditions were run to facilitate crack initiation. A visual inspection was performed before each change in torque. Some conclusions are

1. The most effective metrics (in decreasing order) were M6A*, FM4*, and NB4. They were sensitive enough to pick up the damage while not being overly sensitive to the torque fluctuations.
2. Some metrics such as RMS, Energy Ratio, Energy Operator, Kurtosis, and NA4 are very sensitive to torque fluctuations and thus may not be effective.
3. Accelerometer, location and orientation appear to be critical in effectively detecting the damage early.
4. Despite examining the gear with a 60X microscope, it was not possible to detect whether a tooth crack was occurring, even when some of the metrics indicated that one might exist.

REFERENCES

1. Rose, H. John. "Vibration Signature and Fatigue Crack Growth Analysis of a Gear Tooth Bending Fatigue Failure," Proceedings, 44th Meeting of the Mechanical Failures Prevention Group, Virginia Beach, Virginia, April 1990.
2. Cameron, B.G., "Final Report on CH-46 Aft Transmission Seeded Fault Testing," Westland Research Paper, RP907, September 1993 (Volumes I and II).
3. Farnault, B., Genoux, G., Greco, E., Hebert, Ch., "Damage Progression in Gear Boxes. Test Management," Twenty First European Rotorcraft Forum, Saint Petersburg, Russia, August–September 1995.
4. Nachtsheim, Philip R., "Detecting Tooth Damage in Geared Drive Trains," NASA TM–112207, August 1997.
5. Hess, Andy, Hardman, Bill, Neubert, Chris, "SH-60 Helicopter Integrated Diagnostic System (HIDS) Program Experience and Results of Seeded Fault Testing," 54th Annual Forum, American Helicopter Society, Washington DC, May 1998.
6. Nachtsheim, Philip R., "Analysis of the Effects of Tooth Fracture on the Vibration Characteristics of a Helicopter Main Rotor Transmission," NASA/TM—98-112232, July 1998.

7. Zakrajsek, James J.; Handschuh, Robert F.; Decker, Harry J., "Application of fault detection techniques to spiral bevel gear fatigue data," NASA TM–106467, ARL–TR–345.

8. Decker, Harry J.; Handschuh, Robert F.; Zakrajsek, James J., "An Enhancement to the NA4 Gear Vibration Diagnostic Parameter," NASA TM–106553, ARL–TR–389, Presented at 18th Annual Vibration Inst. Mtg., Hershey, PA, June 1994.

9. Townsend, Dennis P.; Zakrajsek, James J.; Handschuh, Robert F., "Evaluation of a Vibration Diagnostic System for the Detection of Spiral Bevel Gear Pitting Failures," NASA TM–107228, ARL–TR–1106, Presented at ASME 7th Intl Power Trans & Gearing Conf, 1996.

10. Decker, H.J., Zakrajsek, J.J., "Comparison of Interpolation Methods as Applied to Time Synchronous Averaging," Proceedings of 53rd Meeting of the Society for Mechanical Failure Prevention Technology, Virginia Beach, VA, NASA/TM—1999-209086, ARL–TR–1960, April 1999.

11. Zakrajsek, J.J., "An Investigation of Gear Mesh Failure Prediction Techniques," NASA TM–102340, AVSCOM TM 89–C–005, November 1989.

12. Swansson, N.S., "Application of Vibration Signal Analysis Techniques to Signal Monitoring," Conference on Friction and Wear in Engineering 1980. Institution of Engineers, Australia, Barton, Australia 1980.

13. Ma, Jun, "Energy Operator and Other Demodulation Approaches to Gear Defect Detection," Proceedings, 49th Meeting of the Society for Mechanical Failure Prevention Technology, Virginia Beach, Virginia, April 1995.

14. Miller, Irwin, Freund, John E., *Probability and Statistics for Engineers 3rd Edition*, Prentice-Hall, Inc., New Jersey, 1985 p. 74.

15. Martin, H.R., "Statistical Moment Analysis as a Means of Surface Damage Detection," Proceedings, 7th International Modal Analysis Conference, Society for Experimental Mechanics, Schenectady, New York, January 1989.

16. Stewart, R.M., "Some Useful Data Analysis Techniques for Gearbox Diagnostics," Report MHM/R/10/77, Machine Health Monitoring Group, Institute of Sound and Vibration Research, University of Southampton, July 1977.

17. Zakrajsek, J.J., Handschuh, R.F., Decker, H.J., "Application of Fault Detection Techniques to Spiral Bevel Gear Fatigue Data," Proceedings, 48th Meeting of the Society for Mechanical Failure Prevention Technology, Wakefield, Maine, April 1994.

18. Decker, H.J., Handschuh, R.F., Zakrajsek, J.J., "An Enhancement to the NA4 Gear Vibration Diagnostic Parameter," NASA TM–106553, ARL–TR–389, June 1994.

19. Warren, N,. Young, J., "Transmission System Stress Analysis of the Model 206A-1/OH058A Helicopter," Bell Helicopter Co. Report No. 206–099–119, 1969.

20. Lewicki, David G., Coy, John J., "Vibration Characteristics of OH-58A Helicopter Main Rotor Transmission," NASA TP–2705, AVSCOM TR 86–C–42, April 1987.

REPORT DOCUMENTATION PAGE

Form Approved
OMB No. 0704-0188

1. AGENCY USE ONLY (*Leave blank*)	2. REPORT DATE	3. REPORT TYPE AND DATES COVERED
	June 2003	Technical Memorandum

4. TITLE AND SUBTITLE

Spiral Bevel Pinion Crack Detection in a Helicopter Gearbox

5. FUNDING NUMBERS

WBS–22–708–87–12
1L161102AF20

6. AUTHOR(S)

Harry J. Decker and David G. Lewicki

7. PERFORMING ORGANIZATION NAME(S) AND ADDRESS(ES)

National Aeronautics and Space Administration
John H. Glenn Research Center at Lewis Field
Cleveland, Ohio 44135–3191

8. PERFORMING ORGANIZATION REPORT NUMBER

E–13922

9. SPONSORING/MONITORING AGENCY NAME(S) AND ADDRESS(ES)

National Aeronautics and Space Administration
Washington, DC 20546–0001
and
U.S. Army Research Laboratory
Adelphi, Maryland 20783–1145

10. SPONSORING/MONITORING AGENCY REPORT NUMBER

NASA TM—2003-212327
ARL–TR–2958

11. SUPPLEMENTARY NOTES

Prepared for the 59th Annual Forum and Technology Display sponsored by the American Helicopter Society, Phoenix, Arizona, May 6–8, 2003. Responsible person, Harry J. Decker, organization code 5950, 216–433–3964.

12a. DISTRIBUTION/AVAILABILITY STATEMENT

Unclassified - Unlimited
Subject Categories: 07 and 37 Distribution: Nonstandard

Available electronically at http://gltrs.grc.nasa.gov

This publication is available from the NASA Center for AeroSpace Information, 301–621–0390.

12b. DISTRIBUTION CODE

13. ABSTRACT ***(Maximum 200 words)***

The vibration resulting from a cracked spiral bevel pinion was recorded and analyzed using existing Health and Usage Monitoring System (HUMS) techniques. A tooth on the input pinion to a Bell OH-58 main rotor gearbox was notched and run for an extended period at severe over-torque condition to facilitate a tooth fracture. Thirteen vibration-based diagnostic metrics were calculated throughout the run. After 101.41 hours of run time, some of the metrics indicated damage. At that point a visual inspection did not reveal any damage. The pinion was then run for another 12 minutes until a proximity probe indicated that a tooth had fractured. This paper discusses the damage detection effectiveness of the different metrics and a comparison of effects of the different accelerometer locations.

14. SUBJECT TERMS	15. NUMBER OF PAGES
Fracture; Gear; HUMS; Diagnostics	17
	16. PRICE CODE

17. SECURITY CLASSIFICATION OF REPORT	18. SECURITY CLASSIFICATION OF THIS PAGE	19. SECURITY CLASSIFICATION OF ABSTRACT	20. LIMITATION OF ABSTRACT
Unclassified	Unclassified	Unclassified	